# Survey of SOFC cathode materials: an extended summary

Jean-Marc. Bassat

Jean-Marc Bassat

# 4 Survey of SOFC cathode materials: an extended summary

## 4.1 General requirements – electronic conductors

The cathode, or oxygen electrode, is a porous layer where the reduction of the oxygen molecules to oxide ions ($O^{2-}$, ORR) takes place:

$$\tfrac{1}{2}\, O_2 + 2e^- \rightarrow O^{2-}$$

Consequently, a high level of electronic conductivity, $\sigma_e$, of the cathode material is required ($\sigma_e \sim 100$ S/cm at the operating temperature). Moreover, the microstructure (especially the porosity) of the electrode is a key parameter to ensure the access of gaseous oxygen to the surface in between the cathode and the electrolyte, where $O^{2-}$ species are available.

Let us summarize here the general requirements for solid oxide fuel cell (SOFC) cathode:

- High electronic conductivity
- High catalytic activity towards oxygen reduction
- Thermal expansion coefficient (TEC) comparable to that of other SOFC components
- Low chemical reactivity towards other materials used in the SOFC
- High thermal stability
- Optimized microstructure, low cost materials, and mechanical strength
- Because the SOFC is operated at high temperatures for long periods, it should be able to withstand repeated thermal cycling

In the case of electronic conductors, the ORR occurs at the interface between the electrode, the electrolyte, and the gaseous phase, and then on the triple contact lines (labeled TPB for triple phase boundaries). Their number has to be as high as possible. To increase the length of the triple contact lines, composites electrodes formed with an electronic conductor (the cathode material) and an ionic conductor (possibly an electrolyte type conductor) are often prepared. It is mandatory that both phases form two percolating networks. Pure electronic materials were first studied, but rapidly MIEC (mixed ionic and electronic conductors) materials as well as composites were considered. This extended summary follows this plan.

With respect to electronic conductors, the strontium-substituted lanthanum manganite (LSM) [1], with very high electronic conductivity (thanks to the mixed valence of manganese, $Mn^{3+}/Mn^{4+}$ with the formation of electronic holes), has been largely studied (including SOEC operations) in combination with YSZ, also in the form of

https://doi.org/10.1515/9783110596281-012

composites (see, for instance, [2–4]). LSM was, for long, the classical SOFC cathode material, at high operating temperatures (900–1,000 °C).

## 4.2 MIEC materials

Unlike pure electronic conductors, materials with MIEC properties [5, 6] allow the incorporation of oxide ions directly in the network and their diffusion occurs through the material.

In this case, the effective area of the cathodic reaction is extended with respect to the first situation; hence, the reaction is delocalized at the overall surface of the cathode, improving the cell performance. The use of cathode materials with MIEC properties has been largely developed over the last few years. There are mainly three kinds of MIEC materials: i) Oxygen-deficient compounds with perovskite-type structure, ii) double perovskites, and iii) oxygen over-stoichiometric materials with Ruddlesden–Popper-type structure.

## 4.3 Oxygen-deficient MIEC materials

### 4.3.1 Perovskites

Among the different materials with the perovskite structure (Fig. 4.1) identified as MIEC conductors, the strontium-substituted cobaltites $La_{1-x}Sr_xCoO_{3-\delta}$ (LSC) have a high ionic conductivity and good catalytic properties with respect to the oxygen reduction reaction (ORR) [7–9]. However, their TEC coefficients are very high with respect to YSZ or CGO. Using the ferro-cobaltites, $La_{1-x}Sr_xFe_{1-y}Co_yO_{3-\delta}$ (LSFC), a good compromise is obtained between the thermomechanical constraints and the ionic properties [10–13]. In the LSFC materials, the electronic conductivity arises thanks to the strontium to lanthanum substitution leading to the mixed valencies, $Fe^{3+}/Fe^{4+}$ and $Co^{3+}/Co^{4+}$. Another consequence is the formation of oxygen vacancies in this 3D network; the under stoichiometry $\delta$ being dependent on the $x$ value as well as on the oxygen partial pressure. The higher $\delta$ and best ionic conductivity (arising from migration of oxygen in the vacant network) values are obtained for Co-rich materials.

Another studied composition as cathode material is $La_{0.6}Sr_{0.4}Fe_{0.8}Ni_{0.2}O_{3-\delta}$ (LSFN).

In Tab. 4.1, the electrical conductivity, TEC, the tracer oxygen diffusion (D*, which is directly related to the ionic conductivity) and surface exchange ($k$*, which characterizes the ability of gaseous oxygen to be reduced at the surface of the material) coefficients of these perovskite materials are compared with the traditional $La_{1-x}Sr_xMnO_{3-\delta}$ (LSM). D* and $k$* values of these MIEC perovskites are higher than those of LSM.

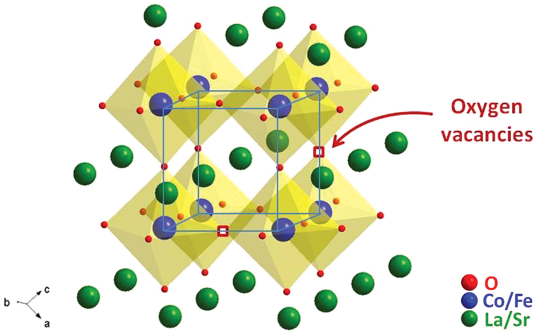


**Fig. 4.1:** Oxygen-deficient perovskite structure.

High TEC values [14–16] compared to those of LSM are evidenced. Another disadvantage of these materials is that they easily form insulating phases such as $La_2Zr_2O_7$ and $SrCoO_3$ at the interface with the YSZ electrolyte, which further degrade the performance of the cell.

**Tab. 4.1:** Comparison of electrical conductivity, TEC, tracer oxygen diffusion (D*) and surface exchange ($k$*) coefficients of some MIEC perovskite materials with LSM.

| Composition | $\sigma_e$ at 900 °C S/cm | TEC, α ($10^{-6}$ $K^{-1}$) | D* at 900 °C ($cm^2$/s) | $k$* at 900 °C (cm/s) |
|---|---|---|---|---|
| LSC | 500–1,500 [17] | 18–26 [18] | $10^{-9}$ ($x = 0.1$)<br>$3 \times 10^{-6}$ ($x = 0.7$) [19] | $10^{-6}$ ($x = 0.1$)<br>$2 \times 10^{-5}$ ($x = 0.7$) [19] |
| LSCF (6428) | 200 [16] | 16 [16] | $5 \times 10^{-8}$ [16] | $7 \times 10^{-7}$ [16] |
| LSFN (6428) | 300 [16] | 14 [16] | $5 \times 10^{-8}$ [16] | $7 \times 10^{-7}$ [16] |
| LSM | 200 [20] | 10–12 [21] | $10^{-13}$ ($x = 2$) [22] | $5 \times 10^{-8}$ ($x = 2$) [22] |

$Ba_{0.5}Sr_{0.5}Co_{0.8}Fe_{0.2}O_{3-\delta}$ (BSCF) can also be used as SOFC cathode materials [23]. Its electronic conductivity is high (~ 30 S/cm at 600 °C) [24], the oxygen diffusion properties interesting ($D^* \sim 5.10^{-7}$ $cm^2$/s and $k \sim 10^{-5}$ cm/s at 600 °C) [25], and the oxygen under stoichiometry high ($\delta \sim 0.3$ at RT) [26]. However, this material is highly sensitive to the presence of $CO_2$. Formation of strontium and barium carbonates at the grains' surfaces is observed, which is detrimental, in particular to the oxygen diffusion properties [27, 28].

## 4.3.2 Double perovskites

Several materials belonging to a family directly derived from the perovskite have recently been studied as $O^{2-}$ – SOFC cathodes; this family is labeled "doubled perovskites"

with general formulation $AA'B_2O_{5+\delta}$ (A = rare earth, A' = alkaline earth metal, B = transition metal). Despite the usual formulation of "$5 + \delta$," these materials can be also considered as oxygen-deficient. A characteristic of such phases is the ordering of the rare earth and alkaline earth metal layers along the (001) axis, leading to a doubling of the *c* parameter with respect to the perovskite with cubic symmetry [29]. As a result of this cationic ordering, the oxygen vacancies are mainly located in the rare-earth layer ($AO_\delta$), and for an oxygen stoichiometry value $\delta \sim 0.5$, they are as well-ordered along the a-axis, leading to a doubling of the *b* parameter [30]. To our knowledge, only cobalt and manganese allow the formation of these compounds. Moreover, the ordering of the cationic layers is induced by a large difference between the rare earth and the alkaline rare earth metal radii; therefore, barium is mainly used, as also rare earths with small radii.

With respect to applications, main studies are focused on cobaltites. Taskin et al. [31–33] performed the first studies on the MIEC properties of these materials. The most studied compositions are $GdBaCo_2O_{5+\delta}$ and $PrBaCo_2O_{5+\delta}$ [32, 34, 35]. However, substitutions (Co–Fe, Co–Ni, and Ba–Sr) enable slight improvement of the electrode performance [36–38]. Currently, the oxygen diffusion values are still under debate; regarding electronic conductivity, a higher value is obtained for $PrBaCo_2O_{5+\delta}$ [29, 39].

## 4.4 Oxygen – over-stoichiometric MIEC materials: the Ruddlesden–Popper (RP) series $A_{n+1}M_nO_{3n+1}$

Compounds belonging to the RP series have the general formulation $A_{n+1}M_nO_{3n+1}$. A is a lanthanide or alkaline-earth metal and M is a transition metal. With respect to *MIEC properties, nickelates have been more investigated than cobaltites, for instance*. The structure can be described by the intergrowth of octahedral layers (perovskite type) with AO layers (NaCl type), where *n* is related to the number of octahedral layers between the AO layers. Figure 4.2 shows the first three terms of the RP series, which are the only known ones at least for the most used transition metals. When $n = \infty$, the perovskite structure is described.

### 4.4.1 $Ln_2NiO_{4+\delta}$ (Ln = La, Pr, and Nd)

With respect to the RP class of materials, the nickelate series $Ln_{n+1}Ni_nO_{3n+1}$ where Ln = La, Pr, and Nd, have gained significant attention in recent years, especially $n = 1$ phases, as alternative cathode materials [34, 39–43]. It has been established that $Ln_2NiO_{4+\delta}$ (Ln = La, Pr and Nd) with $K_2NiF_4$ structure exhibits a large range of oxygen over-stoichiometry. The reported mean values of oxygen over-stoichiometry are 0.16 for $La_2NiO_{4+\delta}$ [44, 45], 0.22 for $Pr_2NiO_{4+\delta}$ [46, 47], and 0.25 for $Nd_2NiO_{4+\delta}$ [48], then

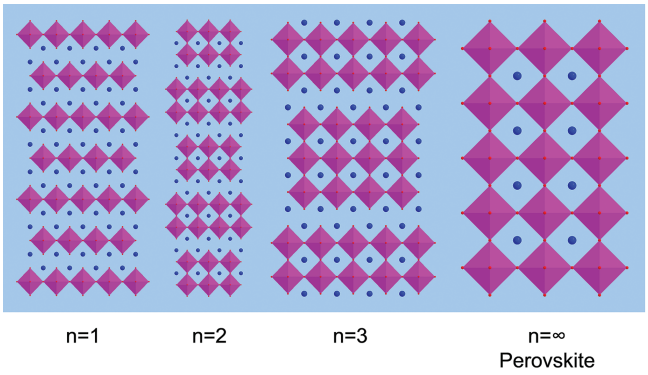


**Fig. 4.2:** Schematic representation of the different structures in the Ruddlesden–Popper series $A_{n+1}M_nO_{3n+1}$, $n = 1, 2, 3, \infty$: ● : A cation, ◆ : M cation, ● : oxygen.

being dependent on the rare-earth size. The oxygen over-stoichiometry $\delta$ value is also dependent upon the synthesis condition for a given composition [49, 50].

The additional (interstitial) oxygen is located in the $Ln_2O_2$ rock-salt interlayer. Moreover, the $NiO_6$ octahedra is elongated along the *c*-axis; hence, three kinds of oxygen are finally distinguished: $O_{apical}$, $O_{equatorial}$, and $O_{interstitial}$ (Fig. 4.3).

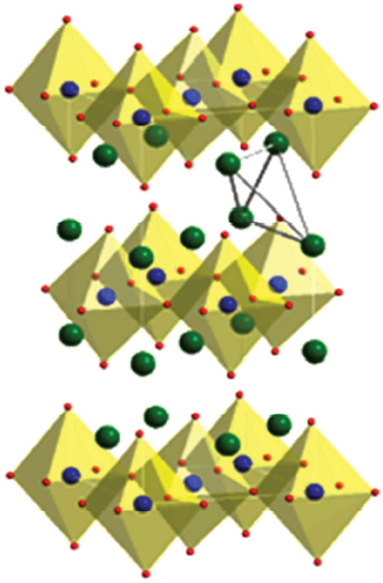

**Fig. 4.3:** Schematic representation of the $Ln_2NiO_{4+\delta}$ structure: ● : nickel, ● : Ln, ● : oxygen (including interstitial oxygen) localized in the Ln cations tetraedra (one is shown).

Thanks to the oxygen over-stoichiometry, a mixed valence ($Ni^{2+}/Ni^{3+}$) appears. The excess oxygen ions and the charge-compensating $Ni^{3+}$ ions (electronic holes) stabilize the $K_2NiF_4$ structure by reducing i) the intrinsic charge separation between the electropositive $Ln_2O_2$ and electronegative $NiO_2$ layers and ii) the structural strain due to the misfit between the $Ln_2O_2$ and $NiO_2$ layers. The Goldschmidt tolerance factor:

$$t = \frac{(r_{Ln} + r_O)}{\sqrt{2}^{*}(r_{Ni} + r_O)}$$

where $r_{Ln}$, $r_O$, and $r_{Ni}$ are the effective ionic radii of $Ln^{3+}$, $O^{2-}$, and $Ni^{2+/3+}$, respectively, helps to predict the stability domains of the various structural varieties (either tetragonal or orthorhombic) of the $K_2NiF_4$ structure.

The oxygen diffusion ($D^*$) and surface exchange ($k^*$) coefficients of these nickelates are among the highest of the known values, especially at intermediate temperatures (about one order magnitude larger than that of conventional perovskites in an intermediate temperature range ($600 < T\ °C < 800$)). For example, the reported $D^*$ values at 600 °C are $1.5 \times 10^{-8}$, $2.5 \times 10^{-8}$, and $7 \times 10^{-9}$ $cm^2/s$ for $La_2NiO_{4+\delta}$, $Pr_2NiO_{4+\delta}$, and $Nd_2NiO_{4+\delta}$, respectively [41, 43, 51]. The ionic conductivity of these materials is directly related to $D^*$ value; hence, the ionic conductivity is the maximum for $Pr_2NiO_{4+\delta}$ [52]. The favored mechanism is probably of the intersticialcy type, involving both apical and interstitial oxygens [53, 54]. Compared to the perovskite materials, the ionic conductivity of the materials considered here has a strong 2D character (about 100 times higher in the ($a$, $b$) plane compared to the $c$-axis direction) [55–57].

The corresponding $k^*$ values at 600 °C are $1 \times 10^{-6}$, $5 \times 10^{-7}$, and $10^{-7}$ cm/s for $La_2NiO_{4+\delta}$, $Pr_2NiO_{4+\delta}$, and $Nd_2NiO_{4+\delta}$, respectively [43]; these characteristics are associated with good electrocatalytic activity and hence the ORR.

Finally, thanks to the mixed valence of nickel and to the oxide-ion conductivity, $Ln_2NiO_{4+\delta}$ materials are mixed ionic and electronic ($O^{2-}/e^-$) conductors, exhibiting good electro-catalytic properties with respect to the ORR.

Hence, these materials are suitable for cathodes in SOFC applications. Up to now, to our knowledge, the best electrochemical result, that is, the lowest polarization resistance ($R_p = 0.1\ \Omega\ cm^2$ at 600 °C), was obtained for $Pr_2NiO_{4+\delta}$ (in symmetrical half-cell configuration $Pr_2NiO_{4+\delta}$//GDC//YSZ [58]). The power density is also maximum, 400 $mW/cm^2$ for $Pr_2NiO_{4+\delta}$ electrode with anode-supported cells [58]. However, chemical stability is an issue for $Pr_2NiO_{4+\delta}$ material [59–61], while $La_2NiO_{4+\delta}$ and $Nd_2NiO_{4+\delta}$ are stable [61, 62] in the 700–900 °C temperature range for up to 72 hours.

### 4.4.2 $Ln_nNi_{n+1}O_{3n+1}$ (Ln = La, Pr, and Nd)

The electronic conductivity of the upper-terms ($n = 2, 3$) of the RP series involving nickel is generally increased with respect to the term $n = 1$ [63–65]. Then, these compositions also attract interest for potential application as cathode for intermediate-temperature (IT)-SOFCs (see, e.g., [66, 67]).

Among the $n = 2$ members, $Ln_3Ni_2O_{7-\delta}$ ($Ln$ = La, Pr, Nd), till date, only $La_3Ni_2O_{7-\delta}$ could be prepared in a phase-pure form, while $Pr_3Ni_2O_{7-\delta}$ and $Nd_3Ni_2O_{7-\delta}$ have been observed only as disordered intergrowths in the corresponding $n = 3$ members [65]. Several studies have investigated the electrode performance of RP-type lanthanum nickelates with conflicting results. Using impedance spectroscopy on symmetric cells with $La_{0.9}Sr_{0.1}Ga_{0.8}Mg_{0.2}O_{3-\delta}$ as electrolyte, Amow et al. [68] found the area-specific resistance (ASR) in the temperature range of 500–900 °C following a trend $La_4Ni_3O_{10-\delta} < La_3Ni_2O_{7-\delta} < La_2NiO_{4+\delta}$. This trend is consistent with that of the cell performance of $La_{n+1}Ni_nO_{3n+1}$/SDC/Ni–SDC cell configurations [69]. However, such a trend was not observed in a comparative study on symmetric cells by Woolley et al. [70]. Sharma et al. [67] have shown that $La_3Ni_2O_{7-\delta}$ would be a better cathode material than $La_4Ni_3O_{10-\delta}$ based on the ASR data of symmetric cells using GCO ($Ce_{0.9}Gd_{0.1}O_{2-\delta}$) as the electrolyte. Increasing the order of RP nickelates promotes the electrical conductivity and the long-term stability at 600–800 °C [68, 69, 71, 72]. In a paper by Vibhu et al. [71], an anode-supported (Ni-YSZ//YSZ) single cell including GDC//$Pr_4Ni_3O_{10+\delta}$ co-sintered electrode showed a maximum power density of 1.60 W/cm$^2$ at 800 °C and 0.68 W/cm$^2$ at 700 °C.

In a recent paper by Song et al. [73], an increase of the electronic $p$-type conductivity of the RP phases with the order parameter $n$ was observed. Moreover, the RP phases display remarkable similarity in their values for the oxygen surface exchange coefficients $k_{chem}$, despite differences in structural order and the type of lanthanide ion. Their oxygen self-diffusion coefficients, $D_s$, calculated from the corresponding values of $D_{chem}$, using data of oxygen non-stoichiometry, are found to profoundly decrease with the order parameter $n$. Note that significant oxygen hypo-stoichiometry is found in the higher order RP phases in contrast to the oxygen hyper-stoichiometry found in the $n = 1$ members.

Finally, apart from material composition, again the microstructure of the cathodes plays a key role in their performance [71].

## 4.5 Composites (prepared by infiltration)

As the ionic conductivity of the ionic conductors (YSZ, Gd doped ceria . . .) is larger than that of the MIECs, the use of composite MIEC/electrolyte is still of interest as shown, for instance, by Laberty et al. [74] who measured the high power density for

a composite cathode made of $La_2NiO_{4+\delta}$ and $Sm_{0.2}Ce_{0.8}O_{1.9}$ (SDC). SOFC developers have, for many years, used composite materials to improve the performance of the anode; however the use of composite cathodes is a more recent innovation. Dusastre et al. [75] wrote a full review paper. The usual preparation route of composites is by ball milling the two materials in an appropriate ratio, prior to their coating (by screen-printing, for example) and sintering on the electrolyte. However, among the fabrication techniques of the composite electrodes, infiltration of a porous ceramic backbone by a solution of cation salts has recently raised growing interest in the SOFC community. This interest is due to the fact that infiltrated cathodes display lower polarization resistances and better robustness to long-term ageing. With this technique, only the backbone is deposited by screen-printing and sintered at high temperature. The catalyst is then infiltrated into the porous backbone and generally annealed at lower temperature. Detailed overviews of electrodes made by infiltration are reported in two reviews from Vohs and Gorte [76], and Ding *et al.* [77].

More precisely, two strategies are developed: 1) Infiltration of an ionic conductor in a porous backbone made of cathode material, and 2) the infiltration of a (MIEC) material in a porous backbone made of ionic conductor. The second strategy is the more used one.

### 4.5.1 Infiltration of an ionic conductor in a porous cathode backbone

This route was applied to LSM, mainly using infiltration of LSM by GDC by San Pin Jiang [78, 79]. Several others studies evidenced the efficiency of this approach when infiltrating SDC in LSM [80–85]. Sc-doped SDC and Pr-doped ceria were infiltrated in YSZ/LSM [86, 87], while LSM was infiltrated by doped $Bi_2O_3$ [88]. MIEC backbones such as LSCF by SDC have also been infiltrated [89].

Table 4.2 sums up the main results using this approach, including the infiltration using metallic catalysts.

### 4.5.2 Ionic conductor backbones infiltrated with electronic/MIEC conductors

The second strategy is the opposite of the first one. The ionic conductor backbone is sintered at high temperature in the first step prior to the infiltration and annealing of the cathode material in a separate step performed at limited temperature. This strategy avoids the chemical reactivity between the two materials. For instance, Armstrong et al. measured very high power densities on a YSZ-based cell infiltrated with LSC: 2.1 W/cm$^2$ at 800 °C [92].

**Tab. 4.2:** Summary of the electrochemical performances obtained when infiltrating a cathode material with an ionic conductor or metallic catalyst.

| Backbone | Infiltrated material | Refs | Measurement $T°$ (°C) | Performance before infiltration | Performance after infiltration |
|---|---|---|---|---|---|
| LSM | GDC | [78] | 850 | $R_p = 7.7\ \Omega{\cdot}cm^2$ | $R_p = 0.5\ \Omega{\cdot}cm^2$ |
| LSM | GDC | [79] | 700 | $R_p = 11.7\ \Omega{\cdot}cm^2$ | $R_p = 0.21\ \Omega{\cdot}cm^2$ |
| LSM | SDC | [80] | 700 | $R_p = 5.4\ \Omega{\cdot}cm^2$ | $R_p = 0.23\ \Omega{\cdot}cm^2$ |
| | | [82] | 600 | – | $P_{max} = 203\ mW/cm^2$ |
| | | [83] | 600 | $P_{max} = 52\ mW/cm^2$ | $P_{max} = 334\ mW/cm^2$ |
| | | [84] | 600 | $P_{max} = 90\ mW/cm^2$ | $P_{max} = 400\ mW/cm^2$ |
| | | [85] | 700 | $R_p = 30\ \Omega{\cdot}cm^2$ | $R_p = 0{,}2\ \Omega{\cdot}cm^2$ |
| YSZ/LSM | LSM-SDC | [86] | 700 | $R_p = 5\ \Omega{\cdot}cm^2$ | $R_p = 0{,}08\ \Omega{\cdot}cm^2$ |
| YSZ/LSM | $Ce_{0.8}Pr_{0.2}O_{2-\delta}$ | [87] | 700 | $R_p = 5\ \Omega{\cdot}cm^2$ | $R_p = 1.3\ \Omega{\cdot}cm^2$ |
| LSM | $(Y_{0.25}Bi_{0.75})_2O_3$ | [88] | 600 | $R_p = 85.2\ \Omega{\cdot}cm^2$ | $R_p = 1.08\ \Omega{\cdot}cm^2$ |
| LSCF | SDC | [89] | 700 | $R_p = 0.4\ \Omega{\cdot}cm^2$ | $R_p = 0.17\ \Omega{\cdot}cm^2$ |
| LSCF | $La_2NiO_{4+\delta}$ | [90] | 700 | $R_p = 1.3\ \Omega{\cdot}cm^2$ | $R_p = 0.04\ \Omega{\cdot}cm^2$ |
| YSZ/LSM | Pd | [91] | 750 | $P_{max} = 0.2\ W/cm^2$ | $P_{max} = 1.42\ W/cm^2$ |

The polarization resistance measurements, $R_p$, performed on symmetrical cells and the power densities on complete cells are given.

**Tab. 4.3:** Summary of the electrochemical performances obtained when infiltrating ionic conductors.

| Backbone | Infiltrated phase | Refs | Measurement $T°$ (°C) | Performance after infiltration |
|---|---|---|---|---|
| GDC | LSC | [93] | 600 | $R_p = 0.044\ \Omega{\cdot}cm^2$ |
| YSZ | LSF | [94] | 700 | $R_p = 0.1\ \Omega{\cdot}cm^2$ |
| GDC | LSCF | [95] | 600 | $R_p = 0.24\ \Omega{\cdot}cm^2$ |
| YSZ | LSC | [92] | 800 | $P_{max} = 2.1\ W/cm^2$ |
| YSZ | LSM | [96] | 650 | $P_{max} = 0.27\ W/cm^2$ |
| LSGM | LSM | [95] | 800 | $P_{max} = 1.4\ W/cm^2$ |
| SDC | $Sm_{0,5}Sr_{0,5}CoO_{3-\delta}$ | [97] | 600 | $P_{max} = 0.95\ W/cm^2$ |

The polarization measurement resistances, $R_p$, performed on symmetrical cells and the power densities on complete cells are given.

A summary of several important results obtained using this strategy is given in Tab. 4.3.

As a final and recent result [98, 99], praseodymium nitrate with (un-expected) MIEC properties was infiltrated into Gd doped ceria (GDC) backbone and fired at 600 °C to form a composite oxygen electrode $Pr_6O_{11}$/GDC. Electrochemical measurements show very low polarization resistance, $R_p = 0.028\ \Omega\ cm^2$ at 600 °C. A single cell made of a commercial Ni-YSZ/YSZ half-cell and of the infiltrated cathode is able to deliver a maximum power density of 825 $mW/cm^2$ at 600 °C.

## References

[1] Charpentier P, Fragnaud P, Schleich D, Lunot C, Gehain E. Ionics 1997, 3(1–2), 155–160.
[2] Yang C, Coffin A, Chen F. Int J Hydrogen Energy 2010, 35(8), 3221–3226.
[3] Ji Y, Kilner JA, Carolan MF. Solid State Ionics 2005, 176, 937.
[4] Kim-Lohsoontorn P, Brett D, Laosiripojana N, Kim Y-M, Bae J-M. Int J Hydrogen Energy 2010, 35, 3958–3966.
[5] Kleitz M, Petitbon F. Solid State Ionics 1996, 92(1–2), 65–74.
[6] Siebert E, Hammouche A, Kleitz M. Electrochim Acta 1995, 40(11), 1741–1753.
[7] Sehlin S, Anderson H, Sparlin D. Solid State Ionics 1995, 78, 235–243.
[8] Petrov A, Kononchuk O, Andreev A, Cherepanov V, Kofstad P. Solid State Ionics 1995, 80, 189.
[9] Berenov A, Atkinson A, Kilner J, Bucher E, Sitte W. Solid State Ionics 2010, 181, 819–826.
[10] Skinner S, Kilner J. Mater Today 2003, 6, 30–37.
[11] Petric A, Huang P, Tietz F. Solid State Ionics 2000, 135, 719–725.
[12] Hashimoto S-I, Fukuda Y, Kuhn M, Sato K, Yashiro K, Mizusaki J. Solid State Ionics 2010, 181, 1713–1719.
[13] Carter S, Selcuk A, Chater R, Kajda J, Kilner J, Steele B. Solid State Ionics 1992, 53–56, 597–605.
[14] Kostogloudis G, Ftikos C. Solid State Ionics 1999, 126(1), 143–151.
[15] Kharton V, Viskup A, Bochkov D, Naumovich E, Reut O. Solid State Ionics 1998, 110(1–2), 61–68.
[16] Audinot JN, Ph.D. thesis, Thèse de Doctorat de l'Université de Bordeaux I (1999).
[17] Mineshige A, Kobune M, Fujii S, Ogumi Z, Inaba M, Yao T, Kikuchi K. J Solid State Chem 1999, 142(2), 374–381.
[18] Petric A, Huang P, Tietz F. Solid State Ionics 2000, 135(1–4), 719–725.
[19] Van Doorn R, Fullarton I, De Souza R, Kilner J, Bouwmeester H, Burggraaf A. Solid State Ionics 1997, 96(1–2), 1–7.
[20] Ming Q, Nersesyan M, Richardson J, Luss D, Shiryaev A. J Mater Sci 2000, 35(14), 3599–3606.
[21] Sakaki Y, Takeda Y, Kato A, Imanishi N, Yamamoto O, Hattori M, Iio M, Esaki Y. Solid State Ionics 1999, 118(3–4), 187–194.
[22] De Souza R, Kilner J. Solid State Ionics 1998, 106(3–4), 175–187.
[23] Shao Z, Halle S. Nature 2004, 431, 170–173.
[24] Wei B, Lu Z, Li S, Liu Y, Liu K, Su W. Electrochem Solid-State Lett 2005, 8, A428.
[25] Wang L, Merkle R, Maier J, Acarturk T, Starke U. Appl Phys Lett 94.
[26] Bucher E, Egger A, Ried P, Sitte W, Holtappels P. Solid State Ionics 2008, 179, 1032–1035.
[27] Yan A, Maragou V, Arico A, Cheng M, Tsiakaras P. Appl Catal B 2007, 76, 320–327.

[28] Bucher E, Egger A, Caraman G, Sitte W. J Electrochem Soc 2008, 155, B1218.
[29] Maignan A, Martin C, Pelloquin D, Nguyen N, Raveau B. J Solid State Chem 1999, 142, 247–260.
[30] Kim J-H, Manthiram A. Solid State Ionics 2009, 180, 1478–1483.
[31] Taskin A, Lavrov A, Ando Y. Appl Phys Lett 2005, 86, 1–3.
[32] Taskin A, Lavrov A, Ando Y. Phys Rev B Condens Matter Mater Phy 71.
[33] Taskin A, Lavrov A, Ando Y. Prog Solid State Chem 2007, 35, 481–490.
[34] Tarançon A, Burriel M, Santiso J, Skinner S, Kilner J. J Mater Chem 2010, 20(19), 3799–3813.
[35] Kim G, Wang S, Jacobson A, Reimus L, Brodersen P, Mims C. J Mater Chem 2007, 17, 2500–2505.
[36] Kim J-H, Prado F, Manthiram A. J Electrochem Soc 2008, 155, B1023–B1028.
[37] Kim J-H, Manthiram A. Electrochim Acta 2009, 54, 7551–7557.
[38] Kim J, Cassidy M, Irvine J, Bae J. J Electrochem Soc 2009, 156, B682–B689.
[39] Zhou Q, Wang F, Shen Y, He T. J Power Sources 2010, 195, 2174–2181.
[40] Kharton V, Viskup A, Naumovkh E, Marques F. J Mater Chem 1999, 9(10), 2623.
[41] Skinner S, Kilner J. Solid State Ionics 2000, 135(1–4), 709–712.
[42] Aguadero A, Fawcett L, Taub S, Woolley R, Wu K-T, Xu N, Kilner J, Skinner S. J Mater Sci 2012, 47(9), 3925–3948.
[43] Boehm E, Bassat J-M, Dordor P, Mauvy F, Grenier J-C, Stevens P. Solid State Ionics 2005, 176 (37–38), 2717–2725.
[44] Bassat J-M, Odier P, Loup JP. J Solid State Chem 1994, 110, 124–135.
[45] Odier P, Bassat J, Rifflet J, Loup J. Solid State Commun 1993, 85(7), 561–564.
[46] Allançon C, Rodriguez-Carvajal J, Fernandez-Diaz M, Odier P, Bassat J, Loup J, Martinez J. Zeitschrift fur Physik B-Condensed Matter 1996, 100, 85–90.
[47] Allançon C, Odier P, Bassat J, Loup J. J Solid State Chem 1997, 131, 167–172.
[48] Fernandez-Diaz M, Martinez J, Rodriguez-Carvajal J. Solid State Ionics 1993, 63–65, 902–906.
[49] Aguadero A, Alonso J, Martinez-Lope M, Fernandez-Diaz M, Escudero M, Daza LD. J Mater Chem 2006, 16(33), 3402–3408.
[50] Demourgues A, Wattiaux A, Grenier J, Pouchard M, Soubeyroux J, Dance J, Hagenmuller P. J Solid State Chem 1993, 105, 458–468.
[51] Skinner S, Kilner J. Ionics 1999, 5(3–4), 171–174.
[52] Boehm E, Les nickelates $A_2MO_{4+\delta}$, nouveaux matériaux de cathode pour piles à combustibles SOFC moyenne température, Ph.D. thesis, ICMCB-CNRS, University of Bordeaux (2002).
[53] Yashima M, Enoki M, Wakita T, Ali R, Matsushita Y, Izumi F, Ishihara T. J Am Chem Soc 2008, 130, 2762–2763.
[54] Minervini L, Grimes R, Kilner J, Sickafus K. J Mater Chem 2000, 10, 2349–2354.
[55] Burriel M, Garcia G, Santiso J, Kilner J, Chater R, Skinner S. J Mater Chem 2008, 18, 416–422.
[56] Bassat J-M, Burriel M, Wahyudi O, Castaing R, Ceretti M, Veber P, Weill I, Villesuzanne A, Grenier J-C, Paulus W, Kilner J. J Phys Chem C 2013, 117, 26466–26472.
[57] Burriel M, Tellez H, Chater RJ, Castaing R, Veber P, Zaghrioui M, Ishihara T, Kilner JA, Bassat JM. J Phys Chem C 2016, 120, 17927.
[58] Ferchaud C, Grenier J-C, Zhang-Steenwinkel Y, Van Tuel M, Van Berkel F, Bassat J-M. J Power Sources 2011, 196(4), 1872–1879.
[59] Kovalevsky A, Kharton V, Yaremchenko A, Pivak Y, Tsipis E, Yakovlev S, Markov A, Naumovich E, Frade J. J Electroceram 2007, 18(3–4), 205–218.
[60] Vibhu V, Flura A, Rougier A, Nicollet C, Grenier JC, Bassat JM. J Energy Chem 2020, 46, 62–70.
[61] Montenegro-Hernandez AB, Vega-Castillo JB, Mogni LB, Caneiro ABC. Int J Hydrogen Energy 2011, 36(24), 15704–15714.

[62] Flura A, Dru S, Nicollet C, Vibhu V, Fourcade S, Lebraud E, Rougier A, Bassat JM, Grenier JC. J Solid State Chem 2015, 228(189).
[63] Greenblatt M. Curr Opin Solid State Mater Sci 1997, 2, 174–183.
[64] Bassat J-M, Allançon C, Odier P, Loup JP, Deus Carvalho M, Wattiaux A. Eur J Solid State Inorg Chem 1998, 35, 173–188.
[65] Zhang Z, Greenblatt M. J Solid State Chem 1995, 117, 236–246.
[66] Tarancon A, Burriel M, Santiso J, Skinner SJ, Kilner JA. J Mater Chem 2010, 20, 19.
[67] Sharma RK, Burriel M, Dessemond L, Bassat J-M, Djurado E. J Power Sources 2016, 325, 337–345.
[68] Amow G, Davidson I, Skinner S. Solid State Ionics 2006, 177, 1205–1210.
[69] Takahashi S, Nishimoto S, Matsuda M, Miyake M. J Am Ceram Soc 2010, 93, 2329–2333.
[70] Woolley RJ, Skinner SJ. J Power Sources 2013, 243, 790–795.
[71] Vibhu V, Rougier A, Nicollet C, Flura A, Fourcade S, Penin N, Grenier J-C, Bassat J-M. J Power Sources 2016, 317, 184–193.
[72] Bannikov DO, Cherepanov J. Solid State Chem 2006, 179, 2721–2727.
[73] Song J, Ning D, Boukamp B, Bassat JM, Bouwmeester HJM. J Mater Chem A 2020, 8, 22206.
[74] Laberty C, Zhao F, Swider-Lyons K, Virkar A. Electrochem Solid-State Lett 2007, 10, B170–B174.
[75] Dusastre V, Kilner JA. Solid State Ionics 1999, 126, 163–174.
[76] Vohs J, Gorte R. Adv Mater 2009, 21, 943–956.
[77] Ding D, Li X, Lai S, Gerdes K, Liu M. Energy Environ Sci 2014, 7, 552–575.
[78] Jiang S, Leng Y, Chan S, Khor K. Electrochem Solid-State Lett 2003, 6, A67–A70.
[79] Jiang S, Wang W. J Electrochem Soc 2005, 152, A1398–A1408.
[80] Xu X, Jiang Z, Fan X, Xia C. Solid State Ionics 2006, 177, 2113–2117.
[81] Zhang L, Zhao F, Peng R, Xia C. Solid State Ionics 2008, 179, 1553–1556.
[82] Tian R, Fan J, Liu Y, Xia C. J Power Sources 2008, 185, 1247–1251.
[83] Chen K, Lü Z, Ai N, Chen X, Hu J, et al. J Power Sources 2007, 167, 84–89.
[84] Chen K, Lü Z, Chen X, Ai N, Huang X, et al. J Power Sources 2007, 172, 742–748.
[85] Ding D, Gong M, Xu C, Baxter N, Li Y, et al. J Power Sources 2011, 196, 2551–2557.
[86] Højberg J, Søgaard M. Electrochem Solid-State Lett 2011, 14, B77–B79.
[87] Ren Y, Ma J, Ai D, Zan Q, Lin X, et al. J Mater Chem 2012, 22, 25042–25049.
[88] Jiang Z, Zhang L, Feng K, Xia C. J Power Sources 2008, 185, 40–48.
[89] Nie L, Liu M, Zhang Y, Liu M. J Power Sources 2010, 195, 4704–4708.
[90] Zhang X, Zhang H, Liu X. J Power Sources 2014, 269, 412–417.
[91] Liang F, Chen J, Jiang S, Chi B, Pu J, et al. Electrochem commun 2009, 11, 1048–1105.
[92] Armstrong T, Rich J. J Electrochem Soc 2006, 153, A515–A520.
[93] Samson A, Søgaard M, Knibbe R, Bonanos N. J Electrochem Soc 2011, 158, B650–B659.
[94] Huang Y, Vohs J, Gorte R. J Electrochem Soc 2004, 151, A646–A651.
[95] Armstrong TV. J Electrochem Soc 2002, 149, A1565–A1571.
[96] Sholklapper T, Lu C, Jacobson C, Visco S, De Jonghe L. Electrochem Solid-State Lett 2006, 9, A376–A378.
[97] Zhao F, Wang Z, Liu M, Zhang L, Xia C, et al. J Power Sources 2008, 185, 13–18.
[98] Nicollet C, Flura A, Vibhu V, Rougier A, Bassat JM, Grenier JC. Int J Hydrogen Energy 2016, 41, 15538–15544.
[99] Guesnet L, Bassat JM, Grenier JC, Chartier T, Geffroy PM. J Eur Ceram Soc 2020, 40, 5662–5669.